Environmental Science Nano

ROYAL SOCIETY OF CHEMISTRY

PAPER

View Article Online
View Journal | View Issue

Cite this: *Environ. Sci.: Nano*, 2022, **9**, 1133

Formation, aggregation, and transport of NOM–Cr(III) colloids in aquatic environments†

Binrui Li,[a] Peng Liao, *[bc] Peng Liu,[a] Dengjun Wang,[d] Zhihang Ye,[a] Jingfu Wang,[b] Jingan Chen,[b] Zigong Ning,[e] Yi Jiang [f] and Chongxuan Liu*[c]

The complexation of natural organic matter (NOM) with chromium (Cr) represents an integral part of Cr cycling in nature. To date, most studies on the interaction of NOM with Cr(III) have focused heavily on the geochemistry of soluble NOM–Cr(III) complexes. However, there is a paucity of information regarding the colloidal chemistry of NOM–Cr(III) particles, which leaves a critical knowledge gap on the fate and colloid-mediated transport of Cr(III) particles. Herein, we explored the formation of NOM–Cr(III) colloids across a wide range of aquatic conditions and quantified their microscopic structures as well as subsequent aggregation and transport behaviors using an array of complementary techniques. Batch results show that the formation and stability of NOM–Cr(III) colloids depend on the C/Cr ratio and NOM source. The concentration and stability of NOM–Cr(III) colloids increase with increasing molar C/Cr ratio. Suwannee river humic acid (SRHA)–Cr(III) colloids are much more stable than Aldrich humic acid (AHA)–Cr(III) colloids, likely due to lower cation bridging and stronger repulsive hydration interactions. Characterization of colloids demonstrates that Cr(III) has six neighboring oxygen atoms in an octahedral geometry and that NOM is relatively enriched on the colloid surface which enhanced the particle stability through electrostatic and steric interactions. Examination of particle stability in natural waters indicates that NOM–Cr(III) colloids can be stable in river waters and groundwaters with low electrolyte concentrations. Results from column studies further confirm that the stable NOM–Cr(III) colloids can be transported readily during advective transport in the porous media. Collectively, these findings provide new mechanistic insights on the formation and stability of NOM–Cr(III) colloids, which are essential for evaluating the long-term fate of Cr and optimizing Cr remediation technology in organic-rich environmental settings.

Received 15th September 2021,
Accepted 23rd January 2022

DOI: 10.1039/d1en00861g

rsc.li/es-nano

Environmental significance

This study provided fundamental molecular-scale and nanoscale understanding of the formation, aggregation, and transport of NOM–Cr(III) colloids in aquatic environments. Although Cr(III) is generally considered to be less mobile under oxic conditions, our findings substantiated that the formation of stable NOM–Cr(III) colloids could lead to associations of Cr(III) with small colloidal particles remaining suspended in water and transporting readily in porous media. We expect that NOM–Cr(III) colloids may be widespread in aquatic environments and that the formation and stability of NOM–Cr(III) colloids could control the fate of Cr. Such findings furnish new insights into the colloid-facilitated transport of Cr(III) which are valuable for understanding Cr cycling processes and remediation strategies in organic-rich aquatic environments.

Introduction

Subsurface chromium (Cr) contamination as a result of industrial activities and geochemical processes poses dire consequences to aqueous ecosystems and drinking water supplies due to toxicity and persistence.[1] The U.S. Environmental Protection Agency (EPA) sets the maximum contaminant level for total Cr in drinking water at 100 μg L^{-1},[2] which includes highly toxic Cr(VI) and less toxic and less

[a] *School of Environment, China University of Geosciences, 388 Lumo Road, Wuhan, 430074, P. R. China*
[b] *State Key Laboratory of Environmental Geochemistry, Institute of Geochemistry, Chinese Academy of Sciences, Guiyang, 550081, PR China. E-mail: liaopeng@mail.gyig.ac.cn*
[c] *State Environmental Protection Key Laboratory of Integrated Surface Water-Groundwater Pollution Control, School of Environmental Science and Engineering, Southern University of Science and Technology, Shenzhen, 518055, P. R. China. E-mail: liucx@sustech.edu.cn*
[d] *School of Fisheries, Aquaculture and Aquatic Sciences, Auburn University, Auburn, AL 36849, USA*
[e] *School of Civil and Environmental Engineering, Harbin Institute of Technology, Shenzhen 518055, China*
[f] *Department of Civil and Environmental Engineering, The Hong Kong Polytechnic University, Hung Hom, Kowloon, Hong Kong, China*
† Electronic supplementary information (ESI) available. See DOI: 10.1039/d1en00861g

mobile Cr(III). Reduction of soluble Cr(VI) to Cr(III) with geochemical reductants can produce $Cr(OH)_3$ ($K_{sp} = 7 \times 10^{-31}$ at 298 K) and other low solubility Cr(III) precipitates (*e.g.*, $Cr_xFe_{1-x}(OH)_3$, $0 < x < 1$) and can be a promising remediation strategy to immobilize contaminants.[3–5] However, the reduced Cr(III) can be mobile when associated with elevated concentrations of complexing ligands in aquifers.[6] Remediation effectiveness and efficiency for Cr are thus determined by not only the rate of Cr(VI) reduction but also the subsequent mobility of reduced Cr(III) products.[4,7] Although Cr(VI) concentration declined to a very low concentration as a result of reductive immobilization, we still need to understand the mobility of Cr(III) since the reduced Cr(III) species could be reoxidized to Cr(VI) when the redox conditions shift to oxidizing conditions.[8–10] Understanding the transport propensity of Cr(III) species is thus fundamentally important for a thorough estimation of the ultimate fate of Cr and the long-term efficiency of the remediation effort.

The geochemistry of Cr(III) is controlled by complexation reactions with natural organic matter (NOM), a heterogeneous mixture of chemically diverse organic macromolecules, which can occur ubiquitously in aquatic environments.[11,12] Cr(III) can intimately bind with functional groups of NOM as a monomeric or a polynuclear NOM–Cr(III) complex,[12] which dominates the solubility and mobility of Cr(III) depending on the solution pH.[13] Mounting field-based studies have reported elevated concentrations of organically complexed Cr(III) that remains soluble in natural waters for extended periods of time under neutral pH conditions.[14–16] Evidence from laboratory studies further revealed that organically complexed Cr(III) constitutes the main products of Cr(VI) biotic/abiotic reduction under organic-rich conditions.[6,17,18] A mechanistic understanding of the transport of NOM–Cr(III) complexes is thus critical for predicting the fate of Cr(III).

Although there is abundant literature on the interactions between NOM and Cr(III),[12,19,20] most of the previous studies have focused on the coordination and oxidation of organic–Cr(III) complexes, and there is limited information regarding the colloidal chemistry of NOM–Cr(III) particles, which constrains our ability to fully evaluate the transport of Cr. Traditional analytical techniques typically treat organic–Cr(III) complexes as dissolved forms using an arbitrary filter membrane (450 or 220 nm pore size) to separate particulates and dissolved (<450 or 220 nm) phases.[17] However, there is increasing evidence that organically complexed metals are colloids with sizes ranging between 1 and 450 nm.[7,13,21] For example, we have recently observed the formation of NOM–Cr(III) colloids (1–220 nm) upon Cr(VI) reduction by reduced NOM under anoxic conditions.[22] Studies have shown that mobile colloids can be considered as a dominant player in facilitating transport of low solubility metals and radionuclides in subsurface environments.[23–25] A prerequisite for NOM–Cr(III) colloid-facilitated transport of Cr(III) is that they should form a stable colloid suspension, which is controlled by the rates of particle aggregation and deposition as established by the Derjaguin–Landau–Verwey–Overbeek (DLVO) theory.[26–28] Aggregation of organic–metal colloids is an important mechanism in modifying the particle size distribution, particle interaction, and, subsequently, in controlling their mass flux, settling and deposition dynamics in aquatic environments.[29–31] Despite much research into the aggregation and deposition of engineered nanoparticles with NOM,[11,32–34] the study on the stability and transport of naturally occurring NOM–Cr(III) colloids is lacking.

Although our recent work reported the formation of NOM–Cr(III) colloids upon Cr(VI) reduction under organic-rich anoxic conditions,[22] there are still several knowledge gaps regarding the microscopic structure, particle stability, and transport of NOM–Cr(III) colloids. The objective of this study was to advance the understanding of the underlying mechanisms controlling the formation, aggregation, and transport of NOM–Cr(III) colloids over a range of environmentally relevant oxic conditions at pH 7. We hypothesize that the concentration ratios of NOM to Cr(III) and the origins of NOM are critical factors influencing the colloidal properties of NOM–Cr(III) particles. We tested and verified these hypotheses using a set of batch experiments to examine the formation and aggregation kinetics of NOM–Cr(III) colloids followed by a set of laboratory-scale column experiments to evaluate the transport of NOM–Cr(III) colloids in a porous medium. We used a variety of techniques to yield insights into the molecular and nanoscale properties of NOM–Cr(III) colloids. We also unraveled the stability of NOM–Cr(III) colloids in real-world waters. Altogether, the new data gained from this study provided a sound basis for accurately predicting the colloid-mediated transport of Cr(III) in organic-rich environmental settings.

Materials and methods

Materials

A Cr(III) stock solution (1.5 g L^{-1}, 28.9 mM) was prepared from $Cr(NO_3)_3{\cdot}9H_2O$. NOM isolates included a terrestrial source of Aldrich humic acid (AHA, 1415-93-6, Sigma-Aldrich) and an aquatic source of Suwannee River humic acid (SRHA, International Humic Substances Society (IHSS)). These humic acids were selected because they are widely used in other colloid chemistry studies,[29,35] so that our experimental findings could be readily compared with previous observations. Stock suspensions of AHA and SRHA were prepared by dissolving aliquots of dried powders in ultrapure water adjusted to pH 10.5 ± 0.1 with 1 M NaOH in the dark for 24 h. The resulting suspensions were filtered through 0.45 μm nitrocellulose membranes (Millipore) under a vacuum and stored at 4 °C in the dark before use. The stock concentration of each NOM was determined as nonpurgeable organic carbon using a total organic carbon (TOC) analyzer (Multi N/C 3100). Additional characteristics are summarized in Table S1 in the ESI.†

Colloid formation

Duplicate experiments were performed in magnetically stirred batch reactors (100 mL) that were shielded with aluminum foil at room temperature (25 ± 0.5 °C) under air-saturated oxic conditions (see Table S2†). The pH was maintained at 7 using 1 M NaOH/HCl without the addition of any buffers. A pH of 7 was selected because it is an environmentally relevant value ubiquitous in aquatic environments.[7,13,30,36] Aliquots of NOM stock suspension were dispensed into the reactors to create a series of NOM working suspensions at concentrations of 0–50 mg C per L for AHA and 0–100 mg C per L for SRHA, respectively. The concentrations of AHA and SRHA were selected to be representative of those found in aquatic environments.[7,29,30,37–40] Then, 10 mg L^{-1} (192.3 μM) of Cr(III) from the stock solution was added to these vigorously stirred suspensions, yielding C/Cr molar ratios of 0–43.3. A relatively high Cr(III) concentration was chosen to improve the analytical sensitivity and accuracy for studying the colloidal stability of organically complexed Cr(III). Actually, high concentrations of organically complexed Cr(III) (*e.g.*, as high as 20 mg L^{-1}) can be present in natural and contaminated aquatic environments.[16,17,41–44] The tested C/Cr molar ratios were selected because they cover a range of C/Cr molar ratios found in sediments and groundwater.[17,43,45,46] Separate control experiments were performed in parallel using NOM alone. The resulting suspensions were continuously and truly mixed with Teflon-coated magnetic stir bars at a speed of 600 rpm for 24 h to reach equilibrium.[7] pH values were measured in the samples collected before, during, and after the reaction using a pH electrode. pH drift was minimal (±0.1 pH unit) over the time course of the experiments. The samples were collected at the termination of the batch experiments for colloid chemistry analysis and for later colloid aggregation experiments.

Aqueous concentrations of Cr(III) and NOM in the NOM–Cr(III) samples were determined based on the following size fractionation: truly dissolved species (<10 kDa, roughly equal to <1–3 nm), small colloids (1–3 to 220 nm), large colloids (220–450 nm), and particulates (>450 nm). In this study, colloids are operationally defined as particles having a size between 10 kDa and 450 nm. Detailed description of the size fractionation is provided in the ESI.† The total Cr concentration in each size fraction was measured by inductively coupled plasma mass spectrometry (ICP-MS) (Agilent 7700 series). Due to the lack of redox reactions between NOM and Cr(III), the Cr(III) concentration was expected to be equal to the total Cr concentration. The NOM concentration in each fraction was determined using a TOC analyzer. Dynamic light scattering (DLS) (Zetasizer Nano, Malvern) was used to measure the particle size distribution of the NOM–Cr(III) suspensions. The same instrument was also used to measure the electrophoretic mobility (EPM), which was subsequently converted to zeta potential using the Smoluchowski approximation.[28] The suspensions were imaged using aberration-corrected ultrahigh-resolution scanning transmission electron microscopy (Cs-corrected STEM) to determine the morphology and microstructural composition of the NOM–Cr(III) colloids. More detailed descriptions of the instrumental analyses are provided in the ESI.†

The selected suspension samples collected at the end of the experiment under steady-state conditions were centrifuged and freeze-dried to yield solids for X-ray absorption spectroscopy (XAS), cryogenic X-ray photoelectron spectroscopy (cryogenic XPS), and attenuated total reflectance Fourier transform infrared (ATR-FTIR) characterization. Details regarding the sample preparation, data collection, and analysis for these instrumental measurements are described in the ESI.† Briefly, Cr K-edge XANES and EXAFS spectra were collected in fluorescence mode on the beamline 20-BM of the Advanced Photon Source (APS) at the Argonne National Laboratory. Cryogenic XPS spectra were collected on a PHI 5000 VersaProbe III SXM scanning X-ray microprobe equipped with a monochromatic Al Kα source at cryogenic temperature (−160 °C). ATR-FTIR spectra were collected using a Thermo Nicolet iS50 FTIR spectrometer with a diamond internal reflection element.

Aggregation kinetics

Time-resolved DLS was used to monitor the aggregation kinetics of the NOM–Cr(III) colloids formed at the completion of the batch experiments. Scattered light was detected at a scattering angle of 90° and the autocorrelation function was accumulated for 15 s. Given the high amount of NOM–Cr(III) precipitates formed at lower C/Cr ratios, we devoted our consideration of aggregation kinetics to those at higher C/Cr ratios in which the suspensions were visually stable (Fig. S1†). Aggregation kinetics of the NOM–Cr(III) colloids were evaluated by the addition of a divalent cation (Ca^{2+} or Mg^{2+}), which decreased the repulsive barrier between the particles, thereby inducing aggregation. Ca^{2+} and Mg^{2+} were selected because they are common species in groundwater and have been shown to play a significant role in the aggregation of natural and engineered colloids.[32,34] For each aggregation kinetic measurement, a predetermined amount of electrolyte stock solution (Ca^{2+} or Mg^{2+}) was quickly pipetted into a cuvette containing an appropriate volume of NOM–Cr(III) colloids at a given molar C/Cr ratio, making a total volume of the final suspension of ~1 mL. After 1.5 s of mixing, the samples were immediately transferred into a DLS chamber to start the measurement. Control aggregation experiments with NOM alone (AHA and SRHA) were performed in the same matrices as the aggregation of the NOM–Cr(III) colloids.

Attachment efficiency (α) was calculated by dividing the initial rate of increase in the hydrodynamic diameter ($D_h(t)$) at a given electrolyte concentration (k) in the reaction-limited aggregation regime by the initial rate of increase in $D_h(t)$ under diffusion-limited (nonrepulsive, k_{fast}) aggregation conditions (eqn 1).[47–49]

$$\alpha = \frac{k}{k_{\text{fast}}} = \frac{\left(\frac{\mathrm{d}}{\mathrm{d}t}D_{\mathrm{h}}(t)\right)_{t\to 0}}{\left(\frac{\mathrm{d}}{\mathrm{d}t}D_{\mathrm{h}}(t)\right)_{t\to 0,\text{fast}}} \quad (1)$$

Colloid stability in natural waters

To support our aggregation kinetic experiments, we performed further stability experiments by investigating the aggregation of NOM–Cr(III) colloids in natural waters. Four groundwater samples and two river water samples were collected from a contaminated tidal Maozhou watershed in Pearl River delta, southern China (see location in Fig. S2†). Selected groundwater was mixed with river water in different ratios (*i.e.*, groundwater : river water = 1 : 1, 1 : 2, 1 : 2.5, and 1 : 3) to create an array of solutions representing groundwater–surface water interactions. A summary of the sampling, preparation, and analysis of the water samples is available in the ESI,† and the measured water chemistry composition is provided in Table S3.† The stability of NOM–Cr(III) colloids was evaluated by dispersing AHA–Cr(III) colloids and SRHA–Cr(III) colloids in each filtered natural water sample to achieve a molar C/Cr ratio of 21.7 and then measuring the *Z*-averaged hydrodynamic diameters over a time period of 1 h using TR-DLS.

Column experiments

Duplicate column experiments were performed to investigate the transport of NOM–Cr(III) colloids and larger particles through sand-packed porous media. Detailed descriptions of the column setup, influent suspension, and quartz sand (model porous media) are described in the ESI.† Briefly, cylindrical Plexiglas columns (2.5 cm diameter, 10 cm length) were wet-packed with 71.4 g of the cleaned quartz sand (median diameter = 0.5 mm), yielding a porosity of 0.47. The NOM–Cr(III) influent suspensions were prepared by adding 10 mg L^{-1} Cr(III) and different concentrations of AHA to stirred, predetermined volumes (500 mL) of filtered river water in the dark, creating molar C/Cr ratios of 1.7 and 21.7. The characteristics of the river water are provided in Table S4.† All the columns were run in an upflow mode using a peristaltic pump at a flow rate of 1 mL min^{-1}, equivalent to 2.94 m per day. After packing, the columns were flushed with 10 pore volumes (PVs) of filtered river water (no NOM–Cr(III) colloids, pH ~ 7) as the background solution to standardize the pore water chemistry. Then, 12 PVs of the NOM–Cr(III) influent suspensions with the same background solution composition were injected into the column, followed by elution with 10 PVs of filtered river water background solution. Bromide (200 mg L^{-1}) as a conservative tracer was fed to the column to determine the hydrodynamic properties of the packed column. Column effluent samples were continuously collected using an automatic fraction collector. At the termination of each transport experiment, the column was disassembled into 10 sections to determine the spatial distribution of Cr(III) retained in the column (see details in the ESI†).

A one-dimensional form of the advection–dispersion equation (ADE) with a two-site kinetic model was used to simulate the transport of the NOM–Cr(III) colloids and larger particles at different molar C/Cr ratios. Details of the model description and parameters are included in section S5 in the ESI.† Colloid filtration theory was also used to evaluate the deposition rate coefficient (k_d) and maximum transport distance (L_{max}) of the NOM–Cr(III) colloids. Detailed parameter descriptions are provided in section S6 in the ESI.†

Results and discussion

NOM–Cr(III) colloid formation

Measurements of the truly dissolved, colloidal, and particulate Cr(III) concentrations following the reaction with AHA and SRHA at pH 7 suggest that no Cr(III) colloids form at C/Cr ≤ 0.9 for AHA–Cr(III) and C/Cr ≤ 4.3 for SRHA–Cr(III) because all the Cr(III) precipitated and became larger particles (Fig. 1a and b). This is consistent with the size fractionation of NOM showing that NOM is associated with larger particles predominantly by adsorption or coprecipitation with Cr(III) (oxyhydr-)oxides (Fig. 1c and d). This is in contrast to control experiments without Cr(III) whereby a larger fraction of NOM occurs in colloidal forms (Fig. S4†). When the molar C/Cr ratio is higher than 1.7 for AHA–Cr(III) and 21.7 for SRHA–Cr(III), the majority (>89%) of Cr(III) and NOM (AHA and SRHA) is present as colloidal forms (10 kDa–450 nm) (Fig. 1a and b).

The prominent precipitation of Cr(III) particles occurring at a low C/Cr ratio in contrast to the colloidal stabilization of Cr(III) particles occurring at a high C/Cr ratio demonstrates that the formation of NOM–Cr(III) colloids depends on the C/Cr ratio. The stabilization of Cr(III) particles in a NOM containing suspension is a balance between the complexation of soluble Cr(III) with NOM and hydrolysis of Cr(III) ions. At a lower C/Cr ratio, a lower AHA and SRHA concentration cannot stabilize the NOM–Cr(III) particles against hydrolysis and precipitation. This can in part be corroborated by zeta potential and light scattering measurements (Fig. 1e and f). Specifically, Cr(III) solid particles generated without NOM are initially positively charged at pH 7. A lower NOM concentration can neutralize and subsequently switch the surface charge of the NOM–Cr(III) particles from positive to slightly negative, causing extensive particle aggregation (Fig. 1e and f), due to the lower intensity of the Coulomb forces.[32] At a higher C/Cr ratio, the surface charge of the NOM–Cr(III) particles is highly negative (Fig. 1f). Further, the *Z*-averaged hydrodynamic diameter of the suspensions is stable, ranging from 70 to 150 nm (Fig. 1e), consistent with size partitioning results. The colloidal Cr(III) concentration observed in this study is several orders of magnitude higher than the expected solubility of $Cr(OH)_3$ solids ($\sim 10^{-9}$ M),[3] supporting the complexation of Cr(III) with NOM in colloidal

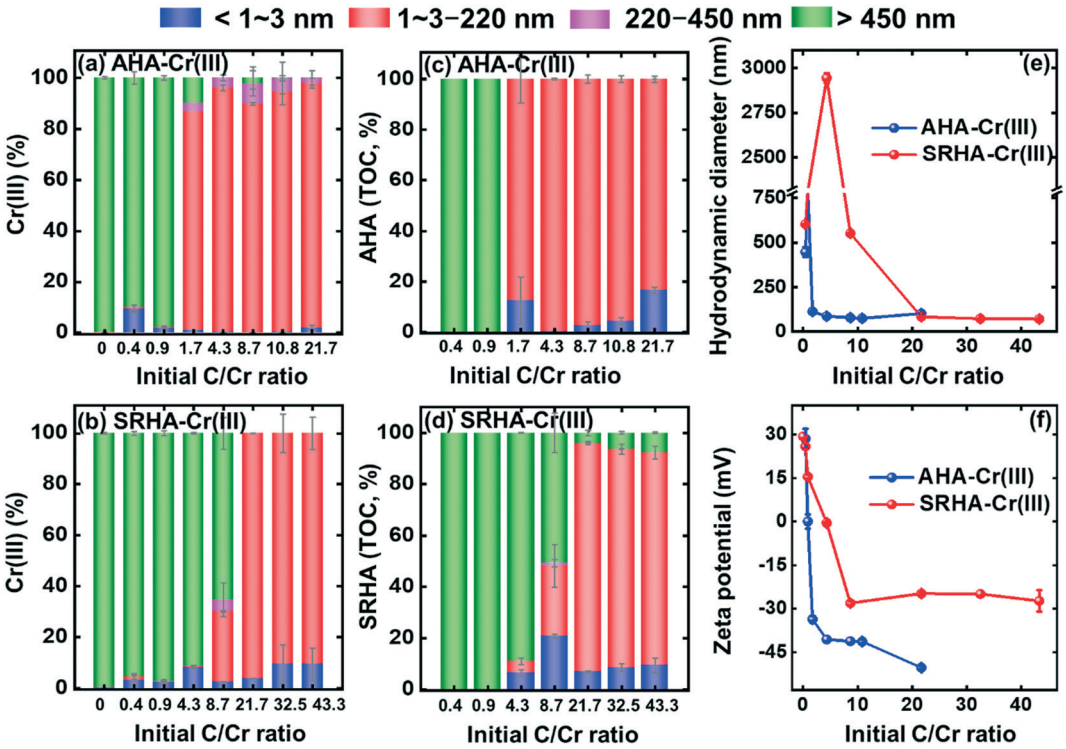

Fig. 1 Percentage of (a and b) Cr(III) and (c and d) NOM concentrations in (a and c) the AHA–Cr(III) suspension and (b and d) SRHA–Cr(III) suspension in different size fractions under steady-state conditions as a function of initial C/Cr molar ratios. The percentage in the *y*-axis means the concentration of (a and b) Cr(III) and (c and d) NOM in a certain size fraction to the total concentration of Cr(III) and NOM in the suspension, so the accumulative concentration percent is equal to 100%. (e) *Z*-Averaged hydrodynamic diameter and (f) zeta potential of the NOM–Cr(III) suspensions under steady-state conditions as a function of initial C/Cr molar ratios. Error bars represent the standard deviations of at least duplicate measurements.

form. This is further confirmed by the close association between colloidal Cr(III) and colloidal NOM ($R^2 > 0.8$, Fig. S5†). The stabilization of the NOM–Cr(III) colloids at a higher C/Cr ratio can be ascribed to the complete complexation of Cr(III) with the negatively charged functional groups that imparted electrostatic and steric effects from adsorbed NOM, which decreased the driving force for precipitation and thus increased the dispersion of the particles.[28,31,32,50]

The source of NOM greatly impacts the formation of NOM–Cr(III) colloids. The observed threshold C/Cr molar ratio for the near complete stabilization of the Cr(III) colloids is much lower in AHA–Cr(III) systems compared to SRHA–Cr(III) systems (C/Cr = 1.7 *vs.* 21.7, Fig. 1a and b). This suggests that AHA has a higher affinity than SRHA for Cr(III) association. The calculated ratio of the average stability constants[51] for Cr(III) bound with soluble NOM to Cr(III) bound with colloidal NOM for AHA–Cr(III) systems is lower than that for SRHA–Cr(III) systems ($K_{Cr(III)-Sol.NOM}/K_{Cr(III)-Coll.NOM}$ = 0.03–0.5 *vs.* 0.1–17.2, see calculation in Fig. S6†). This further supports that AHA has a higher preference for Cr(III) than SRHA for NOM–Cr(III) colloid formation. Such a difference in binding affinity between Cr(III) and different NOM sources may be associated with the differences in the functionality of NOM. NOM contains a variety of functional groups (*e.g.*, carboxyl, carbonyl, phenols, and thiols) with metal-binding affinities spanning several orders of magnitude.[52] Recent studies suggested that Cr(III) binding with NOM mostly occurs at carboxylic sites.[12] Our ATR-FTIR results (Fig. S7†) support this proposition, showing that Cr(III) was predominantly complexed with carboxylic groups through a ligand exchange mechanism (see detailed discussion in section S7†). Compared to SRHA, AHA has a higher carboxyl density and higher aromaticity (Table S1†). The higher binding affinity of AHA to Cr(III) than that of SRHA may be attributable to the higher carboxyl density of AHA.

Cryogenic XPS analysis at different depth profiles enabled the identification of the oxidation state and nanoscale structural information of Cr on the near surface of the NOM–Cr colloids. The spectral results of high-resolution Cr 2p3/2 narrow scans show that Cr(III) dominated across the C/Cr ratios and NOM sources examined (Fig. S8†). The depth profiles of the XPS spectra show that the atomic concentrations of Cr increase with increasing probing depth from the surface to 50 nm depth (Fig. 2, Table S5†). The C/Cr atomic ratios calculated from XPS are statistically higher than the total (initial) C/Cr ratios and colloidal C/Cr ratios (Table S5†). These findings demonstrate the enrichment of NOM on the surface of the NOM–Cr(III) colloids. The observations that the intensity of Cr decreases with increasing initial C/Cr

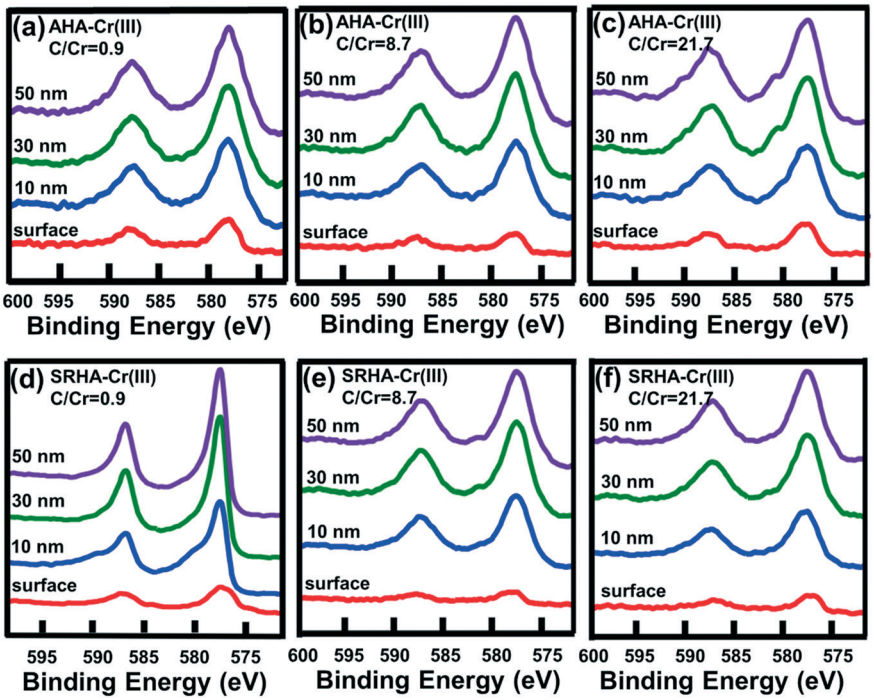

Fig. 2 Cryogenic XPS depth profiling spectra (Cr 2p) of (a–c) the AHA–Cr(III) and (d–f) SRHA–Cr(III) colloids collected at the end of the experiment under steady-state conditions as a function of initial C/Cr molar ratios. All measurements were performed at cryogenic temperature (−160 °C). The samples were ion sputtered using an argon gun operating at 2 kV to determine the surface elemental distribution as a function of probing depth (surface, 10, 30, and 50 nm depth).

ratios at a given probing depth further validate the notion that NOM is heterogeneously distributed within the NOM–Cr(III) colloids with NOM being enriched on the particle surface. Similar observations were also reported for the NOM–Fe(III) colloids.[29] For a given C/Cr ratio, the intensity of Cr in the AHA–Cr(III) colloids is much lower than that in the SRHA–Cr(III) colloids for most of the probing depths (Table S5†), suggesting the higher amount of AHA enriched on the colloid surfaces.

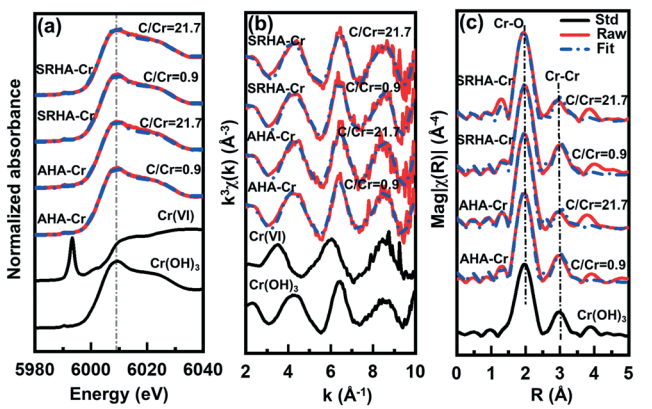

Fig. 3 Cr K-edge (a) XANES, (b) EXAFS, and (c) phase-corrected Fourier-transform EXAFS spectra of the AHA–Cr(III) and SRHA–Cr(III) colloids collected at the end of the experiment under steady-state conditions as a function of initial C/Cr molar ratios. For reference, the patterns of $Cr(OH)_3$ and Cr(VI) are included in the XANES and EXAFS plots.

XAS spectroscopy was further used to quantify the speciation and local molecular coordination environments of Cr within the particle structure. The Cr K-edge XANES spectra show that the Cr in the particles formed at different C/Cr ratios and different NOM sources contain solely Cr(III), as reflected by the absence of any pre-edge band at ~5991 eV (Fig. 3a). This is consistent with the XPS measurements (Fig. 2 and S8†). The first-shell modeling from the Cr K-edge EXAFS spectra indicates that the coordination number of Cr(III) in all the samples ranged from 5.5 to 6.1 with an average Cr(III)–O distance of 1.98 Å (Fig. 3, Table S6†). The measured Cr(III)–O distance is identical to that in previous reports for organically complexed Cr(III) and hydrolyzed Cr(III) ions,[12,53] suggesting that Cr(III) has six neighboring oxygen atoms in an octahedral geometry under all conditions tested. The second Cr–Cr shell modeling revealed that the coordination numbers of Cr(III) observed in the samples at higher C/Cr ratios are smaller compared to samples observed at lower C/Cr ratios (CN = 1.1–1.6 *vs.* 2.1–2.4, Fig. 3c, Table S6†). The smaller coordination numbers of the Cr–Cr shells observed in the samples at higher C/Cr ratios implied the smaller particle sizes or more structural disorder of Cr(III) within the particle structure.[54–56] Such differences in the coordination number of the Cr–Cr bond may be attributed to the fact that the NOM concentration (or C/Cr ratio) could affect the nucleation and polymerization of the NOM–Cr(III) colloids formed at pH 7 in this study. Complexation of Cr(III) by higher NOM concentration may favor smaller particles and inhibit particle aggregation, which is corroborated by the light scattering

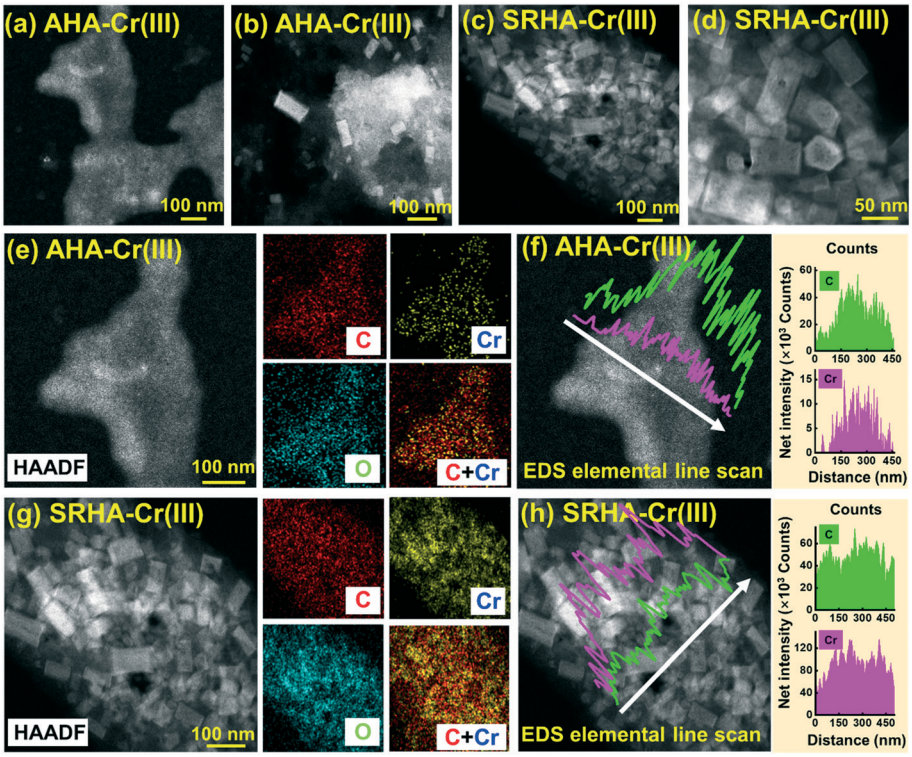

Fig. 4 Morphology and microscopic structure of the NOM–Cr(III) colloids. (a–d) High-resolution HAADF–STEM images of (a and b) the AHA–Cr(III) colloids and (c and d) SRHA–Cr(III) colloids under steady-state conditions. (e and g) High-resolution HAADF–STEM images and the corresponding EDS elemental mapping images of (e) the AHA–Cr(III) colloids and (g) SRHA–Cr(III) colloids. (f and h) High-resolution HAADF–STEM–EDS line-scan profiles recorded through the marked line (white) of (f) the AHA–Cr(III) colloids and (h) SRHA–Cr(III) colloids. Both colloids were imaged at a molar C/Cr ratio of 10.8. All images were taken at a comparable magnification.

measurements and size partitioning results described above (Fig. 1). At a higher C/Cr ratio, the colloids may be present as NOM–Cr(III) binary colloids or NOM-stabilized Cr(III) colloids. However, the EXAFS spectra did not allow us to precisely distinguish these two forms within the resolution of the instrument due to low colloidal mass loading.

To gain more insights into the morphology and microscopic structural features of the NOM–Cr(III) colloids, we performed ultrahigh resolution Cs-STEM–EDS characterization. The morphology of the NOM–Cr(III) colloids was distinguished depending on the source of NOM (Fig. 4a–d). Two types of nanoparticles, which include major flake-like and minor cylindrical-like structures, were observed at random locations in the HAADF–STEM images of the AHA-Cr(III) colloids (Fig. 4a and b). In contrast, the SRHA–Cr(III) colloids only consist of cylindrical-like structures that may be typical for guyanaite particles (Fig. 4c and d). The HAADF–STEM–EDS elemental mappings show that for both colloids, the Cr distribution matched well with that of C across the imaged regions (Fig. 4e and g), confirming the close association between NOM and Cr(III) at the nanoscale. The EDS line scan profiles show that the atomic proportion of C is higher than that of Cr for the AHA–Cr(III) colloids, while the atomic proportion of C is much lower than that of Cr for the SRHA–Cr(III) colloids (Fig. 4f and h and S9†). This difference, combined with the difference in the particle morphology between the AHA–Cr(III) colloids and SRHA–Cr(III) colloids, reinforces the conclusion from XPS that AHA has a higher affinity toward the NOM–Cr(III) colloids over SRHA.

Aggregation of NOM–Cr(III) colloids

Early stage aggregation kinetics of the NOM–Cr(III) colloids in the presence of divalent electrolytes ($CaCl_2$ and $MgCl_2$) was evaluated *via* TR-DLS (Fig. 5 and S10†). The aggregation (stability) behavior of the NOM–Cr(III) colloids delineates distinct reaction-limited (RLCA, unfavorable) and diffusion-limited (DLCA, favorable) regimes within the concentration ranges of $CaCl_2$ and $MgCl_2$ (Fig. 5a, b, d and e), indicating that the particle–particle aggregation of the NOM–Cr(III) colloids is dominated by DLVO type interactions.[34,48,57,58] Water chemistry (*e.g.*, ionic strength; IS) can greatly affect the electrostatic energy by impacting the inverse Debye length (*i.e.*, Debye length $\kappa \propto IS^{0.5}$).[59] At low electrolyte concentrations ($\alpha < 1$), the attachment efficiency increases with increasing Ca^{2+} and Mg^{2+} concentrations, leading to increasing aggregation rates, due to the reduced electrostatic energy barrier between interacting particles, as predicted by the DLVO theory.[28] When the electrolyte concentration exceeds the critical coagulation concentration (CCC) ($\alpha = 1$), a further increase in Ca^{2+} or Mg^{2+} concentration did not increase the aggregation rate because the repulsive energy

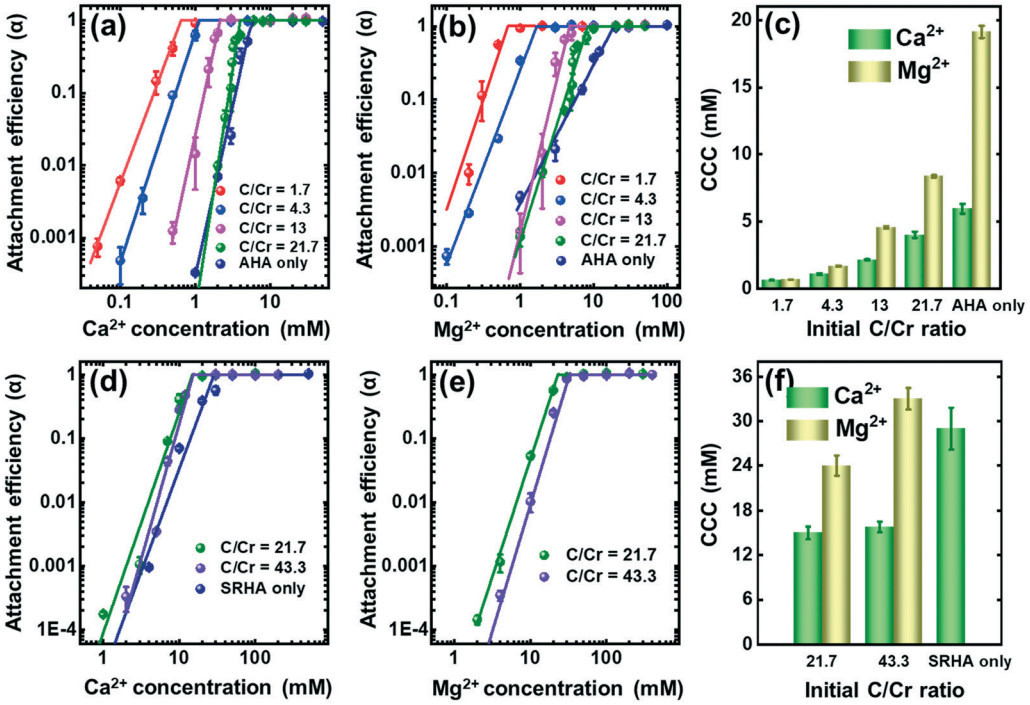

Fig. 5 Attachment efficiency of (a and b) the AHA–Cr(III) colloids and (d and e) SRHA–Cr(III) colloids at different C/Cr molar ratios as a function of concentrations of (a and d) Ca^{2+} and (b and e) Mg^{2+} at pH 7. The corresponding critical coagulation concentration (CCC), which was summarized in panels (c) for the AHA–Cr(III) colloids and (f) for the SRHA–Cr(III) colloids, was derived by intersection of extrapolations through reaction-limited and diffusion-limited regimes as an index of particle aqueous stability. Note that we did not report the Mg^{2+} CCC value for SRHA only (no Cr(III) added) because the SRHA only suspension is still stable even in the presence of 200 mM Mg^{2+}. Error bars represent the standard deviations of duplicate measurements.

barrier was truly eliminated.[60,61] Thus, the CCC value is the minimum concentration of electrolyte required to truly destabilize the colloids, which can be determined from the confluence of extrapolated lines through the RLCA and DLCA regimes.[35] A high CCC value indicates that the colloids have a high degree of particle stability against aggregation.[47,62]

The aggregation of the NOM–Cr(III) colloids is C/Cr ratio dependent. Irrespective of the AHA–Cr(III) colloids and SRHA–Cr(III) colloids, the CCC values, for both $CaCl_2$ and $MgCl_2$ solutions, increase with increasing molar C/Cr ratio (Fig. 5c and f), suggesting that colloids formed at higher C/Cr ratios are less susceptible to aggregation. Enhanced colloidal stability at higher C/Cr ratios may be attributed to the higher amounts of NOM enriched on the particle surface, which alter the surface charge density of colloids in ways that enhance the electrostatic and steric repulsion interactions.[7,13,33,50] Further evidence for this phenomenon can be gained from the zeta potential results (Fig. S11†), which showed that the zeta potential of the NOM–Cr(III) colloids for both $CaCl_2$ and $MgCl_2$ solutions becomes more negative with increasing C/Cr molar ratio. Ca^{2+} exhibited a higher destabilizing capacity than Mg^{2+}, as evidenced by the lower $CaCl_2$ CCC values (Fig. 5), likely due to the stronger complexation and bridging effects of Ca^{2+} relative to Mg^{2+}.[32] Under conditions similar to ours (pH 7), the particle stability of the AHA–Cr(III) colloids observed here is much lower than those of reported AHA–Fe(III) colloids (*e.g.*, $CaCl_2$ CCC = 1.1 mM (C/Cr = 4.3) *vs.* 4.7 mM (C/Fe = 4.7)),[29] which may be related to the lower complexation of Cr(III) to NOM relative to Fe(III).[12]

The SRHA–Cr(III) colloids are much more stable than the AHA–Cr(III) colloids, as they exhibit substantially higher CCC values for both $CaCl_2$ and $MgCl_2$ solutions (Fig. 5c and f and S12 and S13†). The $MgCl_2$ CCC value of the SRHA–Cr(III) colloids is 2.7-times higher than that of the AHA–Cr(III) colloids at the same molar C/Cr ratio of 21.7. Compared to Mg^{2+}, the differences in the CCC values between both colloids appear to decrease with Ca^{2+}. These discrepancies in particle stability between the AHA–Cr(III) colloids and SRHA–Cr(III) colloids can be explained by the differences in the surface chemistry of NOM of different origins. We attribute this discrepancy mainly to the different cation bridging capabilities of AHA and SRHA. As described above, AHA has a higher amount of carboxyl groups compared to SRHA, which is mainly responsible for the bridging with cations such as Ca^{2+} and Mg^{2+}. Further, the higher stability of the SRHA–Cr(III) colloids may be also due to the higher hydrophilicity of SRHA, which contributes to stronger repulsive hydration interactions.[47,63]

Stability of NOM–Cr(III) colloids in natural waters

The aggregation mechanisms described above in simple waters are useful for evaluating the particle stability of the

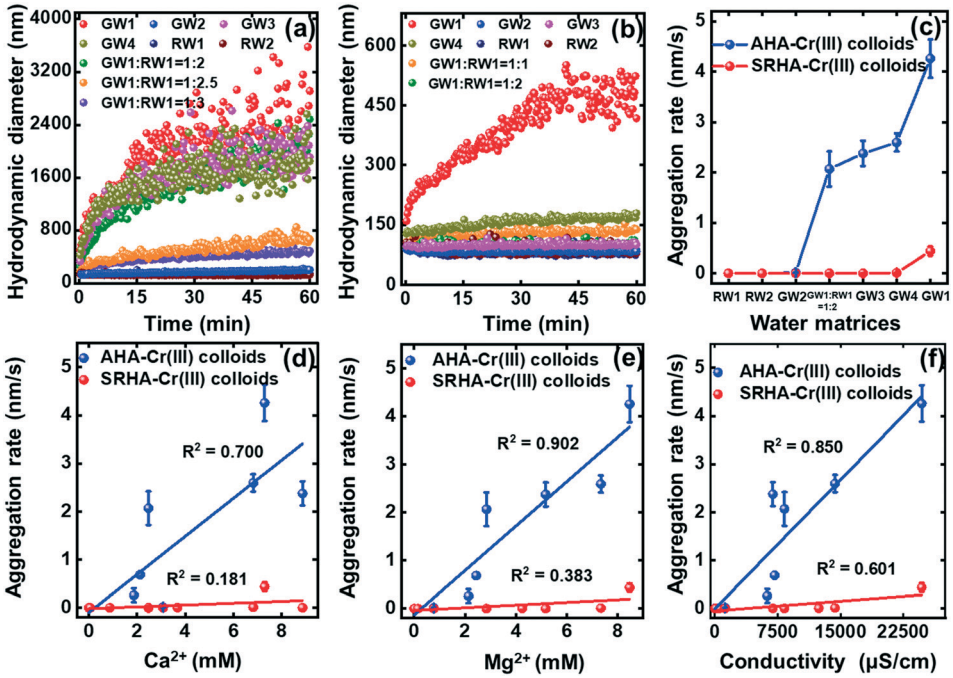

Fig. 6 Stability of the NOM–Cr(III) colloids in natural waters. (a and b) Representative stability profiles of (a) the AHA–Cr(III) colloids and (b) SRHA–Cr(III) colloids in river water, groundwater, and groundwater with river water for different mixtures. (c) The initial aggregation rate of the AHA–Cr(III) colloids and SRHA–Cr(III) colloids under various conditions (the connecting lines are a guide to the eye only). Aggregation rates were quantified from the initially linear increase in hydrodynamic diameter over time. No appreciable aggregation was observed in the absence of the NOM–Cr(III) colloids, reflecting that aggregation is due to the introduction of the NOM–Cr(III) colloids other than other impurities in waters. (d–f) Correlation between the aggregation rate and the (d) Ca^{2+} and (e) Mg^{2+} concentrations as well as (f) conductivity in natural waters. Error bars represent the standard deviations of duplicate measurements.

NOM–Cr(III) colloids in more complex natural waters. In river waters, both the AHA–Cr(III) colloids and SRHA–Cr(III) colloids are essentially highly stable, as they show negligible aggregation over 1 h (Fig. 6a–c). The lack of aggregation is due to the fact that the estimated CCC values for divalent electrolytes (*i.e.*, Ca^{2+} and Mg^{2+}) are considerably higher than the equivalent ionic strength of cations in river waters. For groundwater, negligible aggregation of the AHA–Cr(III) colloids is observed in groundwater (GW2) with lower ionic strength compared to CCC values, while noticeable aggregation is perceived in groundwater samples (GW1, GW3, and GW4) with higher ionic strength relative to CCC values. These observations demonstrate that the estimated CCC value (focused on divalent cations) may be a good indicator of the AHA–Cr(III) colloid stability in natural waters.[64] This is further supported by the positive correlations ($R^2 > 0.7$) between the observed aggregation rates of the AHA–Cr(III) colloids and divalent cation (Ca^{2+} and Mg^{2+}) concentrations in natural waters (Fig. 6d and e). Although there is a substantial amount of dissolved organic carbon (37–50 mg C per L) in groundwater (GW3 and GW4, Table S3†), noticeable aggregation is observed for the AHA–Cr(III) colloids (Fig. 6a), suggesting that dissolved organic carbon may not stabilize the AHA–Cr(III) colloids against aggregation. The aggregation rates of the AHA–Cr(III) colloids in groundwater are substantially higher than those of the SRHA–Cr(III) colloids (Fig. 6c), suggesting the higher stability of the SRHA–Cr(III) colloids, consistent with the aggregation kinetics described before. For GW4, while the Ca^{2+} and Mg^{2+} concentrations are lower than the CCC values for the SRHA–Cr(III) colloids, noticeable particle aggregation is observed (Fig. 6b). This indicates that CCC values alone may not accurately predict the stability of the SRHA–Cr(III) colloids, and other factors such as the ratio of multiple (monovalent/divalent/trivalent) ions would also play a role.[65] The positive correlation ($R^2 > 0.6$) between the aggregation rates and conductivity (Fig. 6f) suggests that the stability of colloids in natural waters is strongly dependent on electrolyte concentrations. To mimic the groundwater–surface water interactions, we mixed the groundwater (GW1) with river water (RW1) at different ratios (GW1 : RW1 = 1 : 1, 1 : 2, 1 : 2.5, and 1 : 3) and found that the aggregation rate of both colloids decreases with decreasing groundwater proportion, confirming that the particle stability is influenced by electrolyte concentrations.

Transport of NOM–Cr(III) colloids

After knowing the formation and aggregation of the NOM–Cr(III) colloids in batch experiments, we attempted to shed light on the transport of the AHA–Cr(III) colloids by monitoring the breakthrough curves and deposition profiles of Cr(III) particles in column experiments (Fig. 7a and b). Mass balance was examined by dividing the amounts of Cr(III)

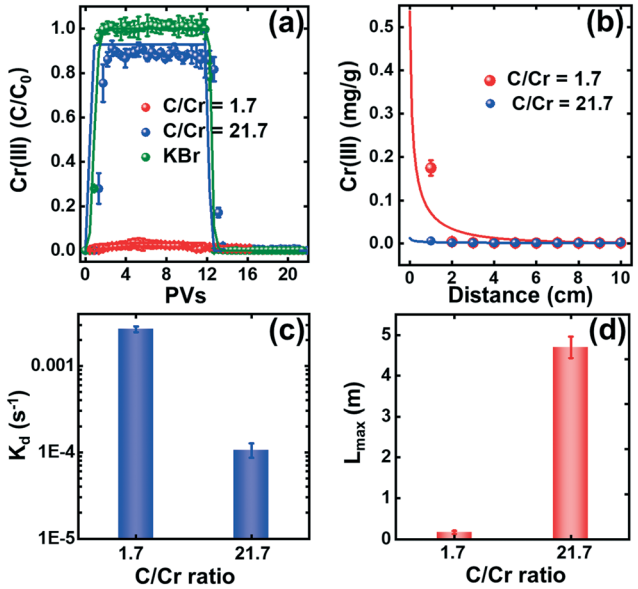

Fig. 7 (a) Breakthrough curves and (b) deposition profiles of Cr(III) from the AHA–Cr(III) colloids and larger particles at molar C/Cr ratios of 1.7 and 21.7 in water-saturated porous media at pH 7.0. The breakthrough curves show the normalized effluent concentration (C/C_0) as a function of pore volume (PV). The fitted curves in panels (a) and (b) were obtained using the two-site kinetic model. (c) The deposition rate coefficient and (d) maximum transport distance of the AHA–Cr(III) colloids and larger particles as a function of C/Cr molar ratios. Error bars represent the standard deviations of duplicate measurements.

in the effluent and those retained in the sand with the total amount of Cr(III) injected into the column (Table S7†). The molar C/Cr ratio has a marked influence on the transport and deposition of Cr(III) particles in porous media. At a low ratio of 1.7, low breakthrough of Cr(III) occurs during the time span of the transport experiments (M_{eff} = 2.7 ± 0.2%, Fig. 7a). This is validated by the undetectable number of particles in the effluent measured by DLS (not shown). The deposition profile further supports that a large portion of Cr(III) is retained in the section adjacent to the column inlet and hyper-exponentially decreased with increasing column depth (Fig. 7b). The observation of a low mass recovery (M_{tot} = 52.4 ± 4.1%) suggests that most Cr(III) precipitated in the influent fitting or tubing as solid phases that were not pumped into the column. Size partitioning results show that the majority (>85%) of Cr(III) in the AHA–Cr(III) influent suspension is present in particulate form (>450 nm) with a negligible colloidal fraction (Fig. S14†). The formation of large particles could enhance collision efficiency due to interception and sedimentation based on the colloid filtration theory.[66,67] Further, straining could narrow down the pore structure due to particle deposition,[68] especially near the column inlet, leading to the observed hyper-exponential deposition profile. Similar observations were also reported for the transport and deposition of engineered carbon nanotube–magnetite nanohybrids in porous media.[69]

In contrast, the AHA–Cr(III) colloids formed at a high C/Cr ratio are highly mobile. The total effluent recovery (M_{eff}) of Cr(III) increased considerably from 2.7 to 85.4% when the C/Cr molar ratio was increased from 1.7 to 21.7, respectively (Fig. 7a). At a molar C/Cr ratio of 21.7, the time for Cr(III) breakthrough (~1.75 PVs) is consistent with the timescale for tracer (KBr) breakthrough under the same conditions, confirming the high mobility of the AHA–Cr(III) colloids in the sand column. Enhanced transport of the AHA–Cr(III) colloids at a high C/Cr ratio may be ascribed to the combined effects of electrostatic and steric repulsions,[21] leading to negligible deposition of the AHA–Cr(III) colloids in the sand. The flat *vs.* hyper-exponential deposition profiles at a higher ratio *vs.* a lower C/Cr ratio, respectively (Fig. 7b), may also be due to enhanced electrostatic and steric stabilization between the AHA–Cr(III) colloids and sand at a higher C/Cr ratio.

The two-site kinetic model can describe the breakthrough curves and deposition profiles of the AHA–Cr(III) colloids. The value of the first-order straining rate coefficient (k_{str}) at a low C/Cr ratio is significantly higher than that obtained at a high C/Cr ratio (2.331 ± 0.212 *vs.* 0.046 ± 0.001 min^{-1}, Table S8†), signifying the importance of straining in governing the transport and deposition of large Cr(III) particles particularly near the column inlet.[70] As expected, the enhanced deposition of larger Cr(III) particles at a low C/Cr ratio resulted in high k_d (2.68 ± 0.2 × 10^{-3} s^{-1}) and low L_{max} (<0.2 m) (Fig. 7c). At a high C/Cr molar ratio of 21.7, the estimated L_{max} was in the order of several meters (~4.7 m) (Fig. 7d), which is a relatively long transport distance, demonstrating the significance of NOM–Cr(III) colloid-facilitated transport of Cr(III) in the porous media.

Environmental implications

This research extends our basic knowledge of the interactions between NOM and Cr(III) by providing molecular-scale and nanoscale insights into the formation, aggregation, and transport of NOM–Cr(III) colloids in aquatic environments. Although Cr(III) is generally considered to be less mobile under oxic conditions,[4] our results demonstrated that the mobility of Cr(III) would be largely enhanced by associating with stable NOM–Cr(III) colloids under organic-rich conditions. Such a process has not been taken into consideration within the conceptual framework of current reactive transport models of Cr in natural systems. Because organically complexed Cr(III) represents an essential part of the Cr cycle,[17] we expect that NOM–Cr(III) colloids may be widespread in aquatic environments and suggest that the fate of Cr can be controlled by the formation and stability of NOM–Cr(III) colloids. As expected, the formation of NOM–Cr(III) colloids in organic-rich systems could lead to more stable associations of Cr(III) with small colloidal particles remaining suspended in the water column and traveling a relatively long distance in the porous media. The formation of stable NOM–Cr(III) colloids causes Cr(III) to be present at concentrations typically higher than the solubility of $Cr(OH)_3$ solids, posing a threat of the reoxidation of Cr(III) to Cr(VI) with naturally occurring oxidants that include manganese

oxides and chloramine disinfectants.[9,10] Further efforts are needed to extend our framework by characterizing the molecular structure and stability of the NOM–Cr(III) colloids and establishing the predictive process-based modeling of colloidal Cr(III) transport in complicated subsurface environments.

Conclusions

This is the first study that provides nanoscale and molecular-scale information to quantitatively elucidate the formation, aggregation, and transport of NOM–Cr(III) colloids in aquatic environments. The integrated findings from complementary measurements (*e.g.*, size partitioning, DLS, ATR-FTIR, cryogenic XPS, XAS, and Cs-STEM) enabled us to conclude that the C/Cr ratio and NOM source affect the formation and stability of NOM–Cr(III) colloids. Specifically, NOM is relatively enriched on the colloid surface which enhanced the particle stability through electrostatic and steric interactions. The relative amount and stability of the NOM–Cr(III) colloids increase with increasing molar C/Cr ratio. SRHA–Cr(III) colloids exhibited much higher aggregation resistance compared to AHA–Cr(III) colloids likely due to lower cation bridging and stronger repulsive hydration interactions. Stability in natural waters shows that the NOM–Cr(III) colloids could be stable in river waters and groundwaters of low electrolyte concentrations, indicating that a significant amount of particles remain suspended and may not be truly removed from these waters. Column results further confirm that the stable NOM–Cr(III) colloids can be transported readily in the porous media, highlighting the importance of colloid-facilitated transport of Cr(III) particles. Overall, our findings provided new insights into the understanding of the fate and transport of NOM–Cr(III) colloids which are valuable for understanding Cr cycling processes and remediation strategies in organic-rich aquatic systems.

Conflicts of interest

There are no conflicts to declare.

Acknowledgements

This study was supported by the Strategic Priority Research Program of Chinese Academy of Sciences (No. XDB40020000), the National Natural Science Foundation of China (No. 42177237 and U1612441), the Program for Guangdong Introducing Innovative and Entrepreneurial Teams (2017ZT07Z479), the Fundamental Research Funds for the Central Universities, China University of Geosciences (Wuhan) (CUGGC06), and the Central Government Leading Local Science and Technology Development QianKeZhongYinDi (20214028). X-ray absorption spectroscopy analyses were performed at Beamlines 20BM of the Advanced Photon Source, Argonne National Laboratory.

References

1 D. Blowes, Tracking hexavalent Cr in groundwater, *Science*, 2002, **295**, 2024–2025.
2 EPA, *National primary drinking water regulations*, Code of Federal Regulations, Title 40, Chapter 1, Subchapter D, Part 141, 2010.
3 B. M. Sass and D. Rai, Solubility of amorphous chromium(III)-iron(III) hydroxide solid solutions, *Inorg. Chem.*, 1987, **26**, 2228–2232.
4 F. C. Richard and A. C. M. Bourg, Aqueous geochemistry of chromium: A review, *Water Res.*, 1991, **25**, 807–816.
5 C. Pan, L. D. Troyer, J. G. Catalano and D. E. Giammar, Dynamics of chromium(VI) removal from drinking water by iron electrocoagulation, *Environ. Sci. Technol.*, 2016, **50**, 13502–13510.
6 I. J. Buerge and S. J. Hug, Influence of organic ligands on chromium(VI) reduction by iron(II), *Environ. Sci. Technol.*, 1998, **32**, 2092–2099.
7 P. Liao, C. Pan, W. Y. Ding, W. L. Li, S. H. Yuan, J. D. Fortner and D. E. Giammar, Formation and transport of Cr(III)-NOM-Fe colloids upon reaction of Cr(VI) with NOM-Fe(II) colloids at anoxic-oxic interfaces, *Environ. Sci. Technol.*, 2020, **54**, 4256–4266.
8 C. N. McClain, S. Fendorf, S. M. Webb and K. Maher, Quantifying Cr(VI) production and export from serpentine soil of the California coast range, *Environ. Sci. Technol.*, 2017, **51**, 141–149.
9 C. Pan, H. Liu, J. G. Catalano, A. Qian, Z. M. Wang and D. E. Giammar, Rates of Cr(VI) generation from $Cr_xFe_{1-x}(OH)_3$ solids upon reaction with manganese oxide, *Environ. Sci. Technol.*, 2017, **51**, 12416–12423.
10 W. Z. Liu, J. Li, J. Y. Zheng, Y. Song, Z. Q. Shi, Z. Lin and L. Y. Chai, Different pathways for Cr(III) oxidation: Implications for Cr(VI) reoccurrence in reduced chromite ore processing residue, *Environ. Sci. Technol.*, 2020, **54**, 11971–11979.
11 G. R. Aiken, H. Hsu-Kim and J. N. Ryan, Influence of dissolved organic matter on the environmental fate of metals, nanoparticles, and colloids, *Environ. Sci. Technol.*, 2011, **45**, 3196–3201.
12 J. P. Gustafsson, I. Persson, A. G. Oromieh, J. W. J. van Schaik, C. Sjöstedt and D. B. Kleja, Chromium(III) complexation to natural organic matter: Mechanisms and modeling, *Environ. Sci. Technol.*, 2014, **48**, 1753–1761.
13 C. Pan, L. D. Troyer, P. Liao, J. G. Catalano, W. Li and D. E. Giammar, Effect of humic acid on the removal of chromium(VI) and the production of solids in iron electrocoagulation, *Environ. Sci. Technol.*, 2017, **51**, 6308–6318.
14 B. R. James and R. J. Bartlett, Behavior of chromium in soils. 5. Fate of organically complexed Cr(III) added to soil, *J. Environ. Qual.*, 1983, **12**, 169–172.
15 A. R. Walsh and J. O'Halloran, Chromium speciation in tannery effluent–I. An assessment of techniques and the role of organic Cr(III) complexes, *Water Res.*, 1996, **30**, 2393–2400.

16 Y. X. Ye, C. Shan, X. L. Zhang, H. Liu, D. D. Wang, L. Lv and B. C. Pan, Water decontamination from Cr(III)-organic complexes based on pyrite/H_2O_2: performance, mechanism, and validation, *Environ. Sci. Technol.*, 2018, **52**, 10657–10664.
17 G. J. Puzon, A. G. Roberts, D. M. Kramer and L. Xun, Formation of soluble organo-chromium(III) complexes after chromate reduction in the presence of cellular organics, *Environ. Sci. Technol.*, 2005, **39**, 2811–2817.
18 X. L. Liu, H. L. Dong, Q. Zeng, X. W. Yang and D. L. Zhang, Synergistic effects of reduced nontronite and organic ligands on Cr(VI) reduction, *Environ. Sci. Technol.*, 2019, **53**, 13732–13741.
19 M. Fukushima, K. Nakayasu, S. Tanaka and H. Nakamura, Chromium (III) binding abilities of humic acids, *Anal. Chim. Acta*, 1995, **317**, 195–206.
20 M. Pettine, F. Gennari, L. Campanella and F. J. Millero, The effect of organic compounds in the oxidation kinetics of Cr(III) by H_2O_2, *Geochim. Cosmochim. Acta*, 2008, **72**, 5692–5707.
21 P. Liao, W. L. Li, D. J. Wang, Y. Jiang, C. Pan, J. D. Fortner and S. H. Yuan, Effect of reduced humic acid on the transport of ferrihydrite nanoparticles under anoxic conditions, *Water Res.*, 2017, **109**, 347–357.
22 B. R. Li, P. Liao, L. Xie, Q. Q. Li, C. Pan, Z. G. Ning and C. X. Liu, Reduced NOM triggered rapid Cr(VI) reduction and formation of NOM–Cr(III) colloids in anoxic environments, *Water Res.*, 2020, **181**, 115923.
23 B. D. Honeyman, Colloidal culprits in contamination, *Nature*, 1999, **397**, 23–24.
24 R. Kretzschmar, M. Borkovec, D. Grolimund and M. Elimelech, Mobile subsurface colloids and their role in contaminant transport, *Adv. Agron.*, 1999, **66**, 121–193.
25 C. Walther and M. A. Denecke, Actinide colloids and particles of environmental concern, *Chem. Rev.*, 2013, **113**, 995–1015.
26 B. V. Derjaguin and L. D. Landau, Theory of the stability of strongly charged lyophobic sols and of the adhesion of strongly charged particles in solutions of electrolytes, *Acta Physicochim. URSS*, 1941, **14**, 633–662.
27 E. J. W. Verwey and J. T. G. Overbeek, *Theory of the Stability of Lyophobic Colloids*, Elsevier, Amsterdam, The Netherlands, 1948.
28 M. Elimelech, J. Gregory, X. Jia and R. Williams, *Particle deposition and aggregation: Measurement, modelling and simulation*, Butterworth-Heinemann, Woburn, MA, 1995.
29 P. Liao, W. L. Li, Y. Jiang, J. Wu, S. H. Yuan, J. D. Fortner and D. E. Giammar, Formation, aggregation, and deposition dynamics of NOM-Iron colloids at anoxic-oxic interfaces, *Environ. Sci. Technol.*, 2017, **51**, 12235–12245.
30 Q. Q. Li, L. Xie, Y. Jiang, J. D. Fortner, K. Yu, P. Liao and C. X. Liu, Formation and stability of NOM-Mn(III) colloids in aquatic environments, *Water Res.*, 2019, **149**, 190–201.
31 M. Sikder, J. J. Wang, B. A. Poulin, M. M. Tfaily and M. Baalousha, Nanoparticle size and natural organic matter composition determine aggregation behavior of polyvinyl pyrrolidone coated platinum nanoparticles, *Environ. Sci.: Nano*, 2020, **7**, 3318–3332.
32 A. Philippe and G. E. Schaumann, Interactions of dissolved organic matter with natural and engineered inorganic colloids: a review, *Environ. Sci. Technol.*, 2014, **48**, 8946–8962.
33 Z. X. Li, S. Shakiba, N. Deng, J. W. Chen, S. M. Louie and Y. D. Hu, Natural organic matter (NOM) imparts molecular-weight-dependent steric stabilization or electrostatic destabilization to ferrihydrite nanoparticles, *Environ. Sci. Technol.*, 2020, **54**, 6761–6770.
34 Z. Q. Tan, Y. G. Yin, X. R. Guo, B. W. Wang, H. P. Shang, J. W. Xu, Q. Zhao, J. F. Liu and B. S. Xing, Natural organic matter inhibits aggregation of few-layered black phosphorus in mono- and divalent electrolyte solutions, *Environ. Sci.: Nano*, 2019, **6**, 599–609.
35 Y. Jiang, R. Raliya, P. Liao, P. Biswas and J. D. Fortner, Graphene oxides in water: assessing stability as a function of material and natural organic matter propterties, *Environ. Sci.: Nano*, 2017, **4**, 1484–1493.
36 P. Liao, K. Yu, Y. Lu, Y. Z. Liang and Z. Q. Shi, Extensive dark production of hydroxyl radicals from oxygenation of polluted river sediments, *Chem. Eng. J.*, 2019, **368**, 700–709.
37 G. Aiken, D. McKnight, R. Wershaw and P. MacCarthy, *Humic substances in soil, sediment, and water: geochemistry, isolation and characterization*, John Wiley & Sons, New York, 1985.
38 E. Tipping, *Cation binding by humic substances*, Cambridge University Press, Cambridge, United Kingdom, 2002.
39 Y. G. Wang, F. M. Michel, Y. Choi, P. J. Eng, C. Levard, H. Siebner, B. H. Gu, J. R. Bargar and G. E. Brown, Pb, Cu, and Zn distributions at humic acid-coated metal-oxide surfaces, *Geochim. Cosmochim. Acta*, 2016, **188**, 407–423.
40 A. Hakim and M. Kobayashi, Aggregation and aggregate strength of microscale plastic particles in the presence of natural organic matter: effects of ionic valence, *J. Polym. Environ.*, 2021, **29**, 1921–1929.
41 G. J. Puzon, R. K. Tokala, H. Zhang, D. Yonge, B. M. Peyton and L. Y. Xun, Mobility and recalcitrance of organo-chromium(III) complexes, *Chemosphere*, 2008, **70**, 2054–2059.
42 G. Lofrano, S. Meric, G. E. Zengin and D. Orhon, Chemical and biological treatment technologies for leather tannery chemicals and wastewaters: A review, *Sci. Total Environ.*, 2013, **461**, 265–281.
43 Y. L. Tang, J. T. Zhao, J. F. Zhou, Y. H. Zeng, W. H. Zhang and B. Shi, Highly efficient removal of Cr(III)-poly(acrylic acid) complex by coprecipitation with polyvalent metal ions: Performance, mechanism, and validation, *Water Res.*, 2020, **178**, 115807.
44 K. Nakayasu, M. Fukushima, K. Sasaki, S. Tanaka and H. Nakamura, Comparative studies of the reduction behavior of chromium(VI) by humic substances and their precursors, *Environ. Toxicol. Chem.*, 1999, **18**, 1085–1090.
45 R. Wadhawan, A. T. Stone and E. J. Bouwer, Biogeochemical controls on hexavalent chromium formation in estuarine sediments, *Environ. Sci. Technol.*, 2013, **47**, 8220–8228.

46 Y. P. Liao, X. B. Min, Z. H. Yang, L. Y. Chai, Q. Liao and B. L. Wu, Assessment of the stability of chromium in remedied soils by Pannonibacter phragmitetus BB and its risk to groundwater, *J. Soils Sediments*, 2014, **14**, 1098–1106.
47 N. Aich, L. K. Boateng, I. V. Sabaraya, D. Das, J. R. V. Flora and N. B. Saleh, Aggregation kinetics of higher-order fullerene clusters in aquatic systems, *Environ. Sci. Technol.*, 2016, **50**, 3562–3571.
48 Y. H. Xu, Q. Ou, C. H. Liu, X. J. Zhou, Q. He, Z. S. Wu, J. Ma, D. M. Lu and X. L. Huangfu, Aggregation and deposition behaviors of dissolved black carbon with coexisting heavy metals in aquatic solution, *Environ. Sci.: Nano*, 2020, **7**, 2773–2784.
49 W. L. Li, C. H. Hinton, S. S. Lee, J. W. Wu and J. D. Fortner, Surface engineering superparamagnetic nanoparticles for aqueous applications: design and characterization of tailored organic bilayers, *Environ. Sci.: Nano*, 2016, **3**, 85–93.
50 M. C. Surette and J. A. Nason, Nanoparticle aggregation in a freshwater river: the role of engineered surface coatings, *Environ. Sci.: Nano*, 2019, **6**, 540–553.
51 J. F. Wu, E. Boyle, W. Sunda and L. S. Wen, Soluble and colloidal iron in the oligotrophic north Atlantic and north Pacific, *Science*, 2001, **293**, 847–849.
52 A. E. Martell and R. D. Hancock, *Metal complexes in aqueous solutions*, Plenum Press, New York, 1996.
53 N. Torapava, A. Radkevich, D. Davydov, A. Titova and I. Persson, Composition and structure of polynuclear chromium(III) hydroxo complexes, *Inorg. Chem.*, 2009, **48**, 10383–10388.
54 G. A. Waychunas, C. S. Kim and J. F. Banfield, Nanoparticulate iron oxide minerals in soils and sediments: unique properties and contaminant scavenging mechanisms, *J. Nanopart. Res.*, 2005, **7**, 409–433.
55 S. S. Mitsunobu, Y. Takahashi, S. Utsunomiya, M. A. Marcus, Y. Terada, T. Iwamura and M. Sakata, Identification and characterization of nanosized tripuhyite in soil near Sb mine tailings, *Am. Mineral.*, 2011, **96**, 1171–1181.
56 M. Q. Zhu, B. Legg, H. Z. Zhang, B. Gilbert, Y. Ren, J. F. Banfield and G. A. Waychunas, Early stage formation of iron oxyhydroxides during neutralization of simulated acid mine drainage solutions, *Environ. Sci. Technol.*, 2012, **46**, 8140–8147.
57 K. L. Chen, S. Mylon and M. Elimelech, Aggregation kinetics of alginate-coated hematite nanoparticles in monovalent and divalent electrolytes, *Environ. Sci. Technol.*, 2006, **40**, 1516–1523.
58 N. B. Saleh, L. D. Pfefferle and M. Elimelech, Aggregation kinetics of multiwalled carbon nanotubes in aquatic systems: measurements and environmental implications, *Environ. Sci. Technol.*, 2008, **42**, 7963–7969.
59 Y. Jiang, R. Raliya, J. D. Fortner and P. Biswas, Graphene oxides in water: correlating morphology and surface chemistry with aggregation behavior, *Environ. Sci. Technol.*, 2016, **50**, 6964–6973.
60 M. Y. Lin, H. M. Lindsay, D. A. Weitz, R. C. Ball, R. Klein and P. Meakin, Universality in colloid aggregation, *Nature*, 1989, **339**, 360–362.
61 A. R. Petosa, D. P. Jaisi, I. R. Quevedo, M. Elimelech and N. Tufenkji, Aggregation and deposition of engineered nanomaterials in aquatic environments: Role of physicochemical interactions, *Environ. Sci. Technol.*, 2010, **44**, 6532–6549.
62 W. L. Li, S. S. Lee, A. M. Mittelman, D. Liu, J. W. Wu, C. H. Hinton, L. M. Abriola, K. D. Pennell and J. D. Fortner, Aqueous aggregation behavior of engineered superparamagnetic iron oxide nanoparticles: effects of oxidative surface aging, *Environ. Sci. Technol.*, 2016, **50**, 12789–12798.
63 F. Xu, C. Wei, Q. Zeng, X. Li, P. J. J. Alvarez, Q. Li, X. Qu and D. Zhu, Aggregation behavior of dissolved black carbon: implications for vertical mass flux and fractionation in aquatic systems, *Environ. Sci. Technol.*, 2017, **51**, 13723–13732.
64 C. Chen and W. Huang, Aggregation kinetics of diesel soot nanoparticles in wet environments, *Environ. Sci. Technol.*, 2017, **51**, 2077–2086.
65 D. X. Zhou and A. K. Arturo, Role of morphology in the aggregation kinetics of ZnO nanoparticles, *Water Res.*, 2010, **44**, 2948–2956.
66 K. M. Yao, M. M. Habibian and C. R. O'Melia, Water and waste water filtration: concepts and applications, *Environ. Sci. Technol.*, 1971, **5**, 1105–1112.
67 N. Tufenkji and M. Elimelech, Correlation equation for predicting single-collector efficiency in physicochemical filtration in saturated porous media, *Environ. Sci. Technol.*, 2004, **38**, 529–536.
68 S. A. Bradford, S. R. Yates, M. Bettahar and J. Simunek, Physical factors affecting the transport and fate of colloids in saturated porous media, *Water Resour. Res.*, 2002, **38**, 1327.
69 D. J. Wang, C. M. Park, A. Masud, N. Aich and S. M. Su, Carboxymethylcellulose mediates the transport of carbon nanotubemagnetite nanohybrid aggregates in water-saturated porous media, *Environ. Sci. Technol.*, 2017, **51**, 12405–12415.
70 D. J. Wang, Y. Jin and D. P. Jaisi, Effect of size-selective retention on the cotransport of hydroxyapatite and goethite nanoparticles in saturated porous media, *Environ. Sci. Technol.*, 2015, **49**, 8461–8470.